PWM-Induced Current Modelling in Stator Slots with Multiple Stacked Coils

Antoine Cizeron, Hugo Milan, Javier Ojeda, Olivier Béthoux

ELECTRIMACS 2022 – Nancy, France, 16th-19th May 2022

PWM-Induced Current Modelling in Stator Slots with Multiple Stacked Coils.

Antoine CIZERON · Hugo MILAN · Javier OJEDA · Olivier BÉTHOUX

Abstract This paper deals with the PWM-induced current and losses in a specific segmented winding structure. The proposed segmentation process enables to split a winding into several coils. These latter are supplied independently by H-bridge converters and are wound around the same magnetic circuit. This process leads to a deeper segmentation of electric drives for enhanced modularity and reduced voltage rating. The strong magnetic coupling between each coil is described, and the control degrees of freedom are presented. This study provides a model based on an analytical method and on an equivalent electrical circuit calibrated through experimental results. A trade-off is found between the losses related either to the distribution of the fundamental component of currents or to the switching power converter supply.

1 Introduction

Electric drive generally involves a power electronics converter associating a DC-link voltage to an electrical machine. In standard EV drive solutions, the voltage rating is between 400 V and 800 V. These voltage values meet the requirements of fast charging and are enabled by the new generation of WBG semi-conductors power components. The implementation of these solutions relies on one high power converter to feed the whole drive. However, the resiliency of this conventional structure is limited, and its power rate implies a separate thermal management for the converter and the electrical machine. Integrated solutions are proposed to bring the power electronics closer to the electrical machine. In these Integrated Modular Motor Drives (IMMD), the power electronics components are spatially distributed around the motor [1]. This is facilitated by the use of multiple elementary converters to supply each portion of the motor winding.

Furthermore, such segmented structure enables the use of low voltage semi-conductor devices, that generally present reduced losses compared to their high voltage counterparts. The various control degrees of freedom available in those segmented structure offer promising opportunities in terms of energy management and resiliency.

The patent proposed in [2] extends the segmentation limit of the motor winding to the turn limit and enables the use of several stacked coils inside the same slots. [3] details the scientific and technical obstacles related to this innovative structure. Recent works like [4] expose the use of a similar structure for an integrated battery charger. In [5], authors combine this kind of segmentation with external coupled inductors to reduce mechanical vibrations. These references only consider balanced current distribution between the different winding sets during the motoring mode. The present paper addresses this issue in a representative geometry. It provides the modelling tools enabling to minimize the losses thanks to uneven current distribution between the different coils.

Each elementary coil being independently supplied, the whole structure presents new control degrees of freedom, these latter were investigated in the particular case of two coils with strong magnetic coupling [6]. A PWM-induced current ripple modelling method is detailed in [7] for conventional synchronous motor. It provides accurate estimation of the current waveforms but is based on an inductance

A. CIZERON · O. BÉTHOUX
GeePs – Université Paris-Saclay, CentraleSupélec, CNRS, Laboratoire de Génie Electrique et Electronique de Paris, 91192, Gif-sur-Yvette, France.
Sorbonne Université, CNRS, Group of Electrical Engineering - Paris, 75252, Paris, France.
e-mail: antoine.cizeron@geeps.centralesupelec.fr

H. MILAN · J. OJEDA
Satie – ENS Paris-Saclay, Laboratory of Systems and Applications of Information and Energy Technologies
4 Avenue des sciences, 91192, Gif-sur-Yvette, France.

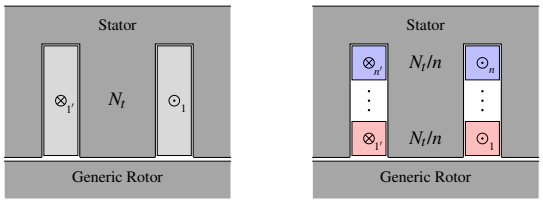

(a) Conventional concentrated winding (b) Concentrated winding with n stacked coils

Fig. 1: Cross section of the proposed winding segmentation within a generic magnetic circuit.

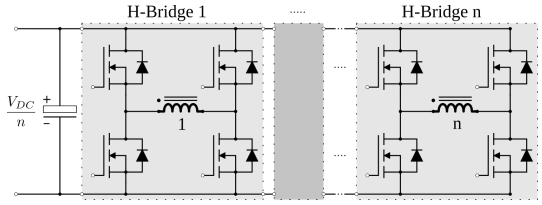

Fig. 2: Segmented supply of the stacked coils.

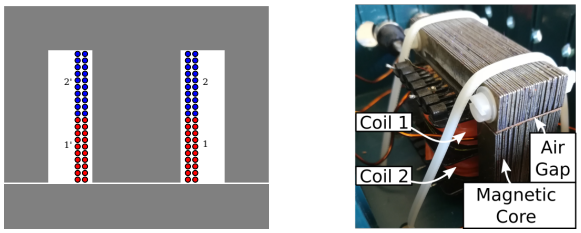

(a) (b)

Fig. 3: a) Geometry of the practical model with two stacked coils and b) the corresponding practical model.

model. Other models are used to understand the PWM-induced losses [8,9] but are not suited for taking into account the new degrees of freedom. Moreover, the influence of the air-gap on the current ripple induced by the Pulse Width Modulation (PWM) in the aforementioned stacked coils has not been yet studied.

This paper emphasizes the link between the control parameters, namely the differential voltages, and the current ripple by modelling two stacked coils within the same magnetic circuit. Measurements are performed to validate the fundamental electrical model and the high frequency model, which estimates the PWM-induced losses over a wide range of operating points. The rest of this paper is structured as follows. Section 2 introduces the concept of the segmentation of ordinary winding into several stacked coils and the case of study. Then, section 3 describes the analytical model applied to the fundamental frequency. Finally, section 4 evaluates the aforementioned trade-off between PWM-induced losses and the losses related to the fundamental distribution of currents in the stacked coils. The last section provides conclusions and perspectives.

2 Stacked coils sharing the same magnetic circuit

2.1 Generic Problem

Fig. 1 shows a generic geometry symbolizing one phase within a concentrated winding arrangement. The conventional winding presents a number of electro-conductive turns written as N_t. These turns are wound around one stator tooth in a concentrated way as shown in Fig. 1a. This winding is then split into n electrically independent coils that are stacked around the same stator tooth.

In the considered structure, each elementary coil is supplied by a low voltage full-bridge converter. This topology can be seen as an extension of the single tooth inverter integration proposed in [10]. Whereas the conventional winding Fig. 1a requires a H-bridge supply with a DC-link voltage V_{DC}, each elementary coil Fig. 1b only requires a H-bridge supply with a reduced DC-link voltage of V_{DC}/n in order to meet the same power rating of the whole structure (Fig. 2). The magnetic circuit was initially designed for the conventional winding. Therefore, the ampere-turns are kept constant to guaranty the proper use of the ferromagnetic material. Thus, the current rating remains the same in both structures since the number of turns per coils is equivalent.

Compared to the conventional supply, the proposed structure presents additional control degrees of freedom since each H-Bridge inverter can be controlled independently. The PWM is used to generate the low frequency voltages applied to each coil. Thus, two frequency bands can be distinguished in this problem

- The Low Frequency band (LF : 0 to 1 kHz) is related to the fundamental frequency of the electrical machine. It corresponds to the back electromotive force (emf) and the fundamental of current in the winding.
- The High Frequency band (HF : $>$ 10 kHz) is related to the PWM signals applied to the winding.

The behaviour of the magnetic circuit and the conductors is different in those two bands. Even if the current magnitude is usually higher in the LF band than in the HF band, [6] has shown that the HF current ripple increase in stacked coils should also be taken into account. Thus two separate models are described, the LF model, based on an analytical method assesses the losses induced by a given current distribution between the stacked coils. Then, it defines the required voltages and so the PWM signals that are injected in the HF model in order to estimate the PWM-induced current ripple.

2.2 Study case of two stacked coils

A practical model was built. It is composed of two stacked coils made of 20 turns each wound around a laminated steel magnetic circuit including an air-gap. Its geometry is detailed in Fig. 3 and used for the analytical model in the LF band. The two coils are supplied either by SI MOSFET H-Bridge converters or linear amplifiers, thus enabling to investigate separately the LF and HF phenomena.

3 LF electrical model and losses assessment

3.1 LF electrical equivalent circuit

Generally, each coil k could be represented as a serial resistance r_k and leakage inductance l_k. One mutual inductance L_m is used for all the stacked coils as they are wound around the same stator tooth. The air-gap ag influences the leakage inductance l_k of each coils. The coil 1 located close to the air-gap barely has no leakage inductance value whereas coil n embraces all the flux lines that are crossing the slot and thus presents the highest leakage inductance value. The serial DC resistance is the same in all coils as they present the same number of turns and thus the same conductor length. This model rely on the fact that it exists two kinds of flux lines. The first contour $\mathscr{C}_{ag}$ corresponds to the flux lines crossing the air-gap vertically (following the y-axis), the other contour $\mathscr{C}_{slot}$ is assumed to cross the slot horizontally (following x-axis). These two paths are represented in Fig. 4a. The induction value in the air-gap and in the slot (between the conductor and the air-gap) can be approximated by:

$$B_{ag} = \frac{\mu_0 \cdot i}{2 \cdot t_{ag}} \quad and \quad B_{slot} = \frac{\mu_0 \cdot i}{w_{slot}} \tag{1}$$

where t_{ag} is the air-gap thickness and w_{slot} is the width of the slot. Thus, for a given position of the conductive turn following y-axis, the inductance can then be computed. The analytical results are compared with the results of a Finite Element Analysis (FEA) method in Fig. 4b, both models are based on the parameters described in Tab. 1. The analytical model represents accurately ($\approx 5\%$ error) the influence of the conductor position on its inductance value according to the FEA results.

3.2 Application to the case of study

The analytical model is used to identify the terms of the LF electrical modelling in the case of two stacked coils (Fig. 3). Considering the computed inductance values of one conductor within the slot (Fig. 4b), the worst case in terms of imbalance corresponds to take the extreme values for the self inductances of stacked coils 1 ($Y = 30$ *mm*) and 2 ($Y =$ 0 *mm*). Since the stacked coils are practically made of 20 turns, the analytical model provides self inductance values $L_1 = l_1 + L_m = 180\ \mu H$ and $L_2 = l_2 + L_m = 220\ \mu H$ (Fig. 5). The two flux paths taken into account leads to consider that all the flux lines embraced by a conductor close to the air-gap are also embraced by any other conductor. In the case of two stacked coils, this leads to set l_1 to zero ($L_1 \approx L_m$) and to admit that the leakage inductance of the coil 2 is the difference between the self inductances : $l_2 = L_2 - L_1 = 40\ \mu H$ while $L_m = 180\ \mu H$.

By supplying successively each stacked coil with a linear amplifier ensuring sinusoidal current, it is possible to identify the inductance and resistance values of the electrical equivalent circuit (Fig. 5). The measured voltages and currents are represented in Fig. 6 and the electrical parameters are reported in Tab. 2. The resistance analytical value is computed taking into account the conductor length and section of the practical model. The results are in close agree-

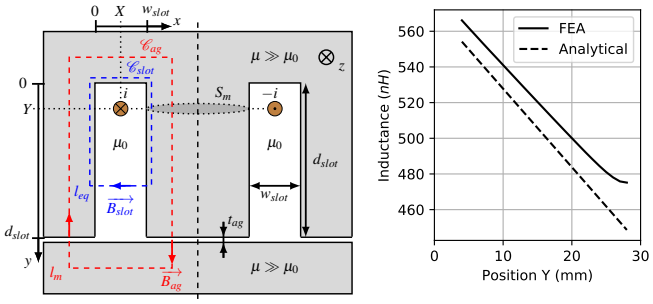

(a) (b)

Fig. 4: a) Analytical model of a generic conductor among a slot and b) comparison of analytical and FEA based inductance value.

Table 1: Geometric parameters of the magnetic core and conductors

Parameter	Symbol	Value
Air-gap thickness	t_{ag} (mm)	0.5
Laminated steel thickness	e_t (mm)	0.5
Number of laminated steel sheet	n_t	35
Magnetic section	S_m (mm²)	350
Average magnetic lenght	l_m (mm)	130
Slot depth	d_{slot} (mm)	30
Slot width	w_{slot} (mm)	10
Vaccum permeability	μ_0 (μH/m)	$4\pi/10$
Copper conductivity	σ (S/m)	$59.6 \cdot 10^6$
Conductor section	S_c (mm²)	1.3
Conductor length	l_c (m)	2.5

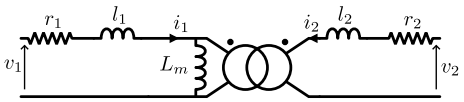

Fig. 5: LF electrical equivalent circuit.

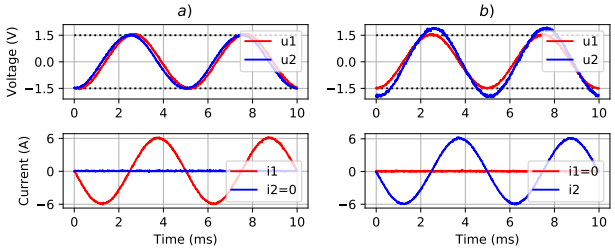

Fig. 6: Voltages and currents measured when only a) coil 1 or b) coil 2 is supplied. 6 A peak current at $f_e = 200\ Hz$.

Table 2: Parameters of the electrical equivalent circuit

Parameter	Analytical value	Experimental value
$r_1 = r_2$	30 $m\Omega$	40 $m\Omega$
$L_1 \approx L_m$	180 μH	200 μH
$l_2 = L_2 - L_m$	40 μH	50 μH

ment, experimental values of inductance are slightly higher than analytical values since the model neglects the inductive part of conductors outside the 2D slot geometry. The resistance measurement used here is not accurate since it is based on the temporal delay observed between u_1 and u_2 in the experimental results (Fig. 6), however, the results are in the same order of magnitude.

The analytical model provide the parameters of the LF equivalent electrical circuit with an appropriate accuracy and enables to estimate the voltages that are ought to be applied to the stacked coils for any current distribution (i_1, i_2). These voltages are then applied to the model that computes the PWM-induced current ripple and losses.

3.3 LF losses assessment

The expression of the induction field values in the slot and air-gap can be used to assess the losses in the two materials, namely the copper conductors and the laminated iron core. Even when multiple conductors are considered, the same flux line paths (Fig. 4a) can be taken into account to compute the induction values between each conductors as in (1). Then, within the coils, the magnetic field is ruled by the following equation:

$$\Delta\vec{H} = \sigma\mu_0 \cdot \frac{\partial\vec{H}}{\partial t} \tag{2}$$

where σ is the copper conductivity. The problem is supposed to have its only dependence following the y-axis. The influence of the position of the conductor within the slot width (following x-axis) is neglected. Equation (2) can then be projected into a 1D problem:

$$\frac{\partial^2 \underline{H}_x}{\partial y^2} = \sigma\mu_0(j\omega)\underline{H}_x. \tag{3}$$

By computing the magnetic field values within each conductors, the current density induced by the flux linkage can be obtained. The losses in the copper are then computed by integrating the square of the current density on the copper volume.

Having the induction values in any position within the slot, the induction in the iron core can be obtained through the conservation of the induction flux. A Steinmetz model is then used to assess the core losses P_{Core} in the geometry for any current distribution. The LF losses are then decomposed into three terms:

$$P_{LF} = P_{Copper,DC} + P_{Copper,supp} + P_{Core} \tag{4}$$

where $P_{Copper,supp}$ corresponds to the additional losses causes by the leakage flux in the slot through the conductors, and $P_{Copper,DC} = R \cdot \left[(i_{1,RMS})^2 + (i_{2,RMS})^2\right]$ corresponds to the losses related to the DC resistance terms of the stacked coils. This latter is not related to the analytical model and strongly depends on the experimental setup serial resistance.

In the LF band, both copper conductors and iron core have frequency dependent behaviour, respectively through the terms $P_{Copper,supp}$ and P_{Core}. These two terms also depend on the current distribution among the several stacked coils. The 20-turns coils are supposed to be arranged in two rows within the slot as Fig. 3a shows. Then, for each stacked coils, 10 conductors having twice the section of a practical conductor are used to represent the 20 turns. Among the LF losses, the terms $P_{Copper,supp}$ and P_{Core} are computed with the analytical model represented in Fig. 4a. The term $P_{Copper,DC}$ is adjusted, taking the estimated value of resistance (30 $m\Omega$) into account.

The two coils are each powered by a dedicated linear amplifier. In this configuration, it is possible to impose the current magnitude in each coil and measure the overall losses related to the fundamental electrical frequency f_e. For several values of fundamental frequency f_e, the total peak current in the slot is fixed at 6 A and several operating points are tested in terms of current distribution between the two stacked coils. The current imbalance varies from -100 % ($i_1 = 0\ A$) to $+100$ % ($i_2 = 0\ A$). The losses computed from (4) are compared to measured results in Fig. 7.

The measured and estimated results are consistent, showing that a positive current imbalance ($i_1 > i_2$) could lead to minimize the LF losses in the magnetic circuit and its stacked coils. At low fundamental frequency, Fig. 7b shows that the experimental optimal current imbalance is mostly due to an eventual resistance disparity and could set to a non zero value. However, when the fundamental frequency increases, the optimal current imbalance clearly shifts toward positive values ($i_1 > i_2$) since the current in coil 1, because of its proximity to the air-gap, induces no induction field in the slot around the conductors of coil 2. However, this result is obtained under a linear power supply and has to be confirmed under PWM excitation.

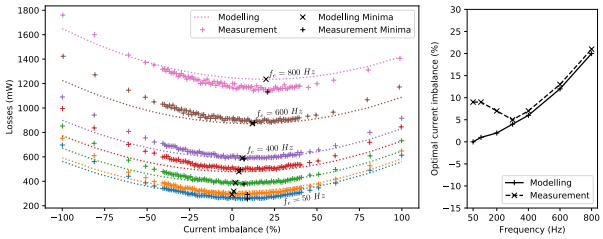

(a) (b)

Fig. 7: a) Measured and estimated LF losses versus current imbalance for several fundamental frequency values f_e and b) Current imbalance minimizing LF Losses.

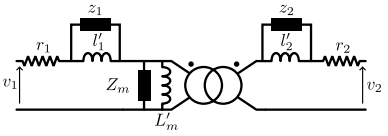

Fig. 8: PWM-induced current modelling of the two stacked coils.

4 Investigation of the control degrees of freedom on the PWM-induced losses

4.1 PWM harmonic based model:

In order to reproduce the PWM-induced current ripple in stacked coils, the LF model is not sufficient. In the HF band, the copper conductors and the iron core present non negligible skin effect. Thus the inductive term is degraded and an additional impedance may be added in parallel to each inductive term to reflect the HF losses in those materials. This is visible on Fig. 8. The impedance z_k represents the additional losses in the copper, which is directly related to the HF leakage inductance l'_k. Impedance Z_m symbolizes the core losses related to the HF mutual inductive term L'_m. Considering the geometry and the frequency of the PWM excitation, an FEA method would require a refined mesh leading to high computation time. Admittance analysis can be used to observe the frequency dependent behaviour of the coils but is not accurate to estimate the current ripple and PWM-induced losses [6]. Therefore, experimental results are used here for the identification of the HF model parameters.

Practically, each of these terms depend on the LF operating point where the switching period occurs. However, in order to simplify this aspect and make rapid conclusions, this dependency is neglected. It is then assumed that this HF model is valid for any switching period based on the hypothesis of magnetic material linearity.

Voltages and HF currents are measured on the practical model with its two H-bridge supply (Fig. 9). The model described in Fig. 10 is calibrated on experimental waveforms of PWM-induced current ripples due to duty-cycle differences ($\Delta\alpha = \alpha_1 - \alpha_2 \neq 0$). The obtained model precisely reproduces the current ripples and provides an estimation of losses (Fig. 9). Using this modelling, it is possible to compute the HF losses due to any duty-cycle configuration (α_1, α_2).

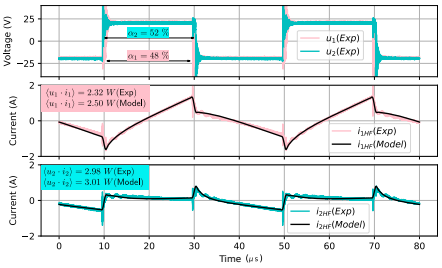

Fig. 9: Measured (colored) and estimated (black) PWM-induced current ripple for $\Delta\alpha = 4\ \%$.

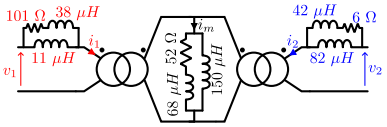

Fig. 10: PWM-induced current modelling of the two stacked coils. The values are calibrated through experimental measurements at fixed duty-cycle.

In this way, the voltages provided by the LF model are applied to the stacked coils in order to meet a given current distribution. The duty-cycles used in each H-bridge are determined for any switching period. At each switching period, the voltages signals are generated from a centred PWM method. The harmonic component of these signals are then treated by the HF model in order to reproduce the PWM-induced current ripple. For each LF current distribution, the required duty-cycle values are used to assess the average HF losses over a fundamental period $1/f_e$. The combination of these two models thus enables to estimate the PWM-induced losses required to reach a given current distribution. The total losses are computed with

$$P_{tot} = P_{Copper,DC} + P_{Copper,supp} + P_{Core} + P_{HF} \quad (5)$$

where P_{HF} is the PWM-induced term averaged over one LF fundamental period. The terms $P_{Copper,supp}$ and P_{Core} are the same than in the LF model (Fig. 7). The losses in inverters are included in $P_{Copper,DC}$. This latter is computed with an equivalent resistance of 220 $m\Omega$. It enables the comparison with the losses measured on the DC-link of the two inverters in the experimental setup.

4.2 Synthesis

For a given Ampere-turn level in the slots, the degrees of freedom offered by the stacked coils enable to consider several current distribution. The measured current waveforms

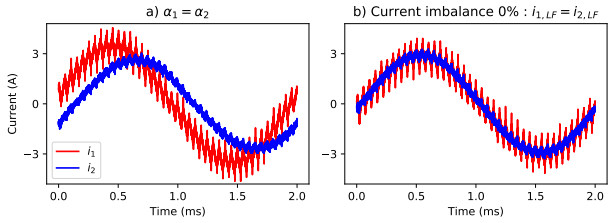

Fig. 11: Measured currents in the stacked coils with LF peak total current : 6 A while maintaining a) equal duty-cycles or b) equal fundamental currents ($\Delta\alpha < 2.5$ %).

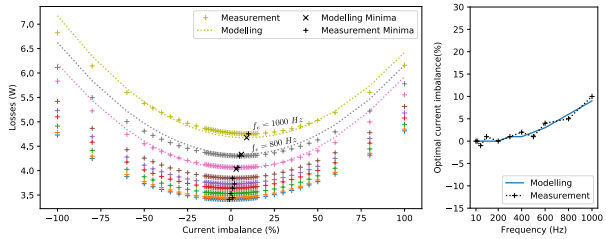

(a) (b)

Fig. 12: a) Measured and estimated total losses P_{tot} versus current imbalance for several fundamental frequency values f_e and b) Current imbalance minimizing the overall losses.

are reported in Fig. 11 showing that the control of the current distribution requires small duty-cycle differences inducing negligible current ripple modifications. The corresponding total losses seen form the DC source are presented in Fig. 12. Similarly to the LF losses (Fig. 7), the minimum of total losses including the PWM-induced losses in the coils and the inverter losses shifts toward positive values when the fundamental frequency f_e increases. It exists a non zero differential currents that minimizes the total losses in the two stacked coils. These minima are reported in Fig. 12b. Thanks to the high coupling between the two stacked coils, small duty-cycle differences (< 5 %) are required to ensure any LF current imbalance. Therefore, the term P_{HF} presents a negligible variation over the different values of current imbalance. The shift of the optimal current imbalance toward positive values is mainly due to LF phenomena represented by $P_{Copper,supp}$ and P_{Core}.

5 Conclusion

The stator winding segmentation studied in this article enables to increase the modularity of the segmented drive and to reduce the voltage rating of the elementary converter. However, the winding configuration obtained presents several coils stacked in the same slots, having then different relative position to the air-gap and strong magnetic couplings. The present papers describes the phenomena involved in these segmented supply and proposes an estimation of the losses depending on the current distribution enforced in the stacked coils. The example of two stacked coils wound around the same magnetic circuit is used to describe the modelling process and an experimental setup provides the necessary information to build the PWM-induced losses model. Finally, non zero differential currents references are investigated in order to mitigate the total losses in the magnetic circuit and conductors. This study is reinforced by taking into account the losses in the several H-bridge converters of the experimental setup. It fully justifies the use of differential currents to properly supply the stacked coils segmented structure at high fundamental frequencies.

References

1. Abdalla Hussein Mohamed, Hendrik Vansompel, and Peter Sergeant. Design of an Integrated DC-Link Structure for Reconfigurable Integrated Modular Motor Drives. *IEEE Transactions on Industrial Electronics*, 0046(c), 2021.
2. E Hoang and E Labouré. Electric machine supplied at low voltage and associated multicellular power train, November 28 2019. US20190363599A1.
3. H Ben Ahmed, L Béthoux, A Cizeron, E Hoang, A Juton, E Labouré, A Mercier, E Monmasson, J Ojeda, L Queval, and G Remy. Electric Traction Chain with Segmented Power Supply. *23rd European Conference on Power Electronics and Applications (EPE21 ECCE Europe)*, September 2021.
4. Qianfan Zhang, Henri Josephson Raherimihaja, Guoqiang Xu, and Xi Zhang. Design and Performance Analysis of Segmented Three-Phase IPMSM for EVs Integrated Battery Charger. *IEEE Transactions on Industrial Electronics*, 68(10):9114–9124, 2021.
5. Wentao Zhang, Yongxiang Xu, Huidong Huang, and Jibin Zou. Vibration reduction for dual-branch three-phase permanent magnet synchronous motor with carrier phase-shift technique. *IEEE Transactions on Power Electronics*, 35(1):607–618, 2020.
6. A Cizeron, J Ojeda, E Labouré, and O Béthoux. Prediction of PWM-Induced Current Ripple in Admittance Analysis. *Energies 2019,12 4418*, 2019.
7. Le Chang and Thomas M. Jahns. Prediction and Evaluation of PWM-Induced Current Ripple in IPM Machines Incorporating Slotting, Saturation, and Cross-Coupling Effects. *IEEE Transactions on Industry Applications*, 54(6):6015–6026, 2018.
8. Le Chang, Woongkul Lee, Thomas M. Jahns, and Jihyun Kim. Comparative analysis of pwm power losses in ipm machines with different modulation schemes using wide-bandgap-based inverters. In *2020 IEEE Energy Conversion Congress and Exposition (ECCE)*, pages 3629–3636, 2020.
9. Davide Cittanti, Vincenzo Mallemaci, Fabio Mandrile, Sandro Rubino, Radu Bojoi, and Aldo Boglietti. Pwm-induced losses in electrical machines: An impedance-based estimation method. In *2021 24th International Conference on Electrical Machines and Systems (ICEMS)*, pages 548–553, 2021.
10. Gerhard Reber, Martin Rittner, Michael Guyenot, Ulrich Kessler, Alexander Klemm, Rainer Holz, and Manfred Reinold. Low-inductive sic h-bridge for direct-inverter-single-tooth-integration (german bmbf public funded research project 'verse'). In *CIPS 2020; 11th International Conference on Integrated Power Electronics Systems*, pages 1–5, 2020.